

## An Application of Potential Vorticity Inversion to Improving the Numerical Prediction of the March 1993 Superstorm

ZONGHUI HUO,\* DA-LIN ZHANG,<sup>†</sup> AND JOHN GYAKUM

*Department of Atmospheric and Oceanic Sciences, McGill University, Montreal, Quebec, Canada*

(Manuscript received 26 January 1996, in final form 28 April 1997)

### ABSTRACT

In this study, a methodology is proposed to improve the model initial conditions, based on available surface temperature observations from ships, buoys, and drifters. It is tested with the numerical prediction of the 12–14 March 1993 superstorm that is initialized at its incipient stage over the Gulf of Mexico. In this methodology, the authors make use of the piecewise potential vorticity (PV) inversion technique and treat the temperature errors at the lowest level as a surrogate PV anomaly. After inverting the wind and mass perturbations from the surface thermal anomaly and its pertinent interior PV anomaly, a three-dimensional, dynamically consistent set of “errors” are obtained and added to the model initial conditions to improve the representation of the lower troposphere over the data-sparse ocean.

It is found that the numerical model prediction, initialized with the modified initial conditions, exhibits significant improvements in the early rapid deepening and the track of the superstorm over ocean, the development of a prefrontal squall line, and the central sea level pressure traces during the life cycle of the cyclone, as verified against observations. These results show that the methodology proposed is promising in improving the representation of lower-tropospheric meteorological variables in the model initial conditions, based on available surface observations over data-sparse regions.

### 1. Introduction

The superstorm of 12–14 March 1993 represents one of the most intense extratropical cyclones that has ever affected the eastern United States and Canada in this century, the so-called storm of the century (Kocin et al. 1995). It was widely perceived as a forecast “success” by the media and general public since the occurrence of this storm was predicted several days in advance by operational models at both the Canadian Meteorological Centre (CMC) and the U.S. National Centers for Environmental Prediction (NCEP). Despite the unprecedented nature of the advanced warnings for the storm, the forecasts were still far from perfect. For example, the operational models initialized at both 0000 and 1200 UTC 12 March 1993 were unable to predict *the initial rapid growth* of the storm over the Gulf of Mexico and the development of a tornado-producing squall line and

its impact on the state of Florida, where the passage of the squall system and cold front caused at least 48 casualties. The total property damages along its path were estimated in excess of \$1.6 billion (Kocin et al. 1995).

In searching for the possible causes for the above-mentioned forecast problems, we investigate both the numerical weather prediction (NWP) models and the model initial conditions. Although the current NWP models are not perfect, they captured well the intensification of the storm during its later stages when it was located over data-dense areas and/or the initial fields contained stronger signals of the cyclonic development—for example, when the models were initialized at and after 0000 UTC 13 March (see Huo et al. 1995). Prior to this time, however, the development signal was weak and the storm was located over the data-sparse region (i.e., the Gulf of Mexico). Therefore, we shift our attention from NWP models to the quality of initial conditions because short-range NWP is partially an initial-value problem.

For this purpose, the model initial conditions are compared with available surface observations from ships, buoys, and drifters over the Gulf of Mexico. It is surprisingly found that the initial low-level thermal field (e.g., the air temperature at 1000 hPa) over the region has been markedly underestimated, as shown in Fig. 1, whereas it conforms reasonably well to the CMC and NCEP analyses over the continent. Furthermore, the sea level pressure (SLP) field over the Gulf of Mexico was

\* Current affiliation: CMRP, University of Oklahoma, Norman, Oklahoma.

<sup>†</sup> Current affiliation: Department of Meteorology, University of Maryland, College Park, Maryland.

*Corresponding author address:* Dr. Da-Lin Zhang, Department of Meteorology, University of Maryland, College Park, MD 20742-2425.

E-mail: dalin@atmos.umd.edu

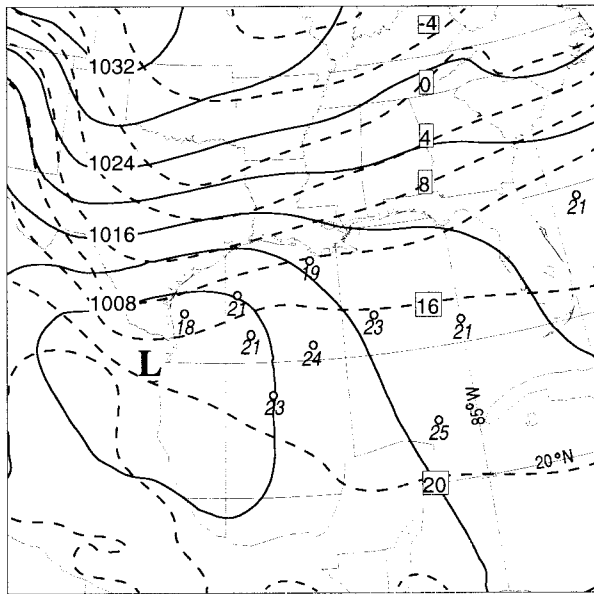


FIG. 1. The model initial conditions: SLP (solid) at intervals of 4 hPa and 1000-hPa temperature (dashed) at intervals of 5°C. The 1000-hPa air temperatures adjusted from the surface observations are also plotted.

roughly 4 hPa higher than the observed and the storm center was displaced about 400 km to the southwest of the analyzed (e.g., see Gilhousen 1994). These errors are typical over the data-void regions. Several possible reasons could be responsible for the underestimation. The CMC global analysis was produced following a 6-h data assimilation cycle (CMC 1995). We have examined the sea surface temperature (SST) analysis and found that it is consistent with the observations over ocean, albeit at a low resolution ( $\sim 100$  km). Therefore, the error may be caused by the planetary boundary layer (PBL) physics, which fail to adjust the lowest levels according to the observed SST during the assimilation. Second, the error may be caused by the analysis algorithm that extrapolates surface observations upward. Although the resulting 1000-hPa temperature analysis may be consistent with the observations, it would not have significant impact on the storm development if the fields were not balanced. Third, the Canadian Regional Finite Element (RFE) model reads the global analysis on standard pressure levels and interpolates/extrapolates it to model  $\sigma$  levels. This process could also produce errors.

The consequences of neglecting these errors are obvious in the present case. First, the underestimation of the low-level temperature and central SLP would slow the initial spinup of the storm. Second, the error in the location of minimum SLP may lead to errors in the prediction of the storm's movement. In particular, the southwestward displacement of the storm center tends to be less favorably "locked" with the upper-level potential vorticity (PV) anomalies, when the associated short-wave disturbances propagate into the region (see

Huo et al. 1995; Kocin et al. 1995). Third, the underestimation of the low-level temperature over the Gulf of Mexico will reduce both the potential moisture content in the maritime PBL and the baroclinicity between the Gulf of Mexico and the southern plain.

Although there are considerable surface (ship or buoys) observations available over the ocean, NWP models tend to either "forget" the surface-layer information quickly or experience some gravitational types of instability if they are simply incorporated without properly modifying the layers above. To use effectively the surface observations, new methods have to be developed so as to improve the representations of the lower troposphere in the model initial conditions. A traditional method is to insert "bogus" soundings based on other available information, including some surface observations, and then force the objective analysis to accept the "bogus" data and adjust the initial fields toward the desired patterns. This approach has been successfully used by many simulation studies (e.g., Anthes et al. 1983; Zhang and Fritsch 1986). Weaknesses of this technique include the subjective nature in the preparation of "bogus" data and the possible introduction of unbalanced flows into the model. Another way to reduce the error is to use appropriate SSTs over a multiday data assimilation cycle and let the model internal physics adjust to the observed SST pattern. In this paper, we propose an alternative method, based on the PV concept (Hoskins et al. 1985) and the piecewise PV inversion technique (Davis and Emanuel 1991), to improve the lower-tropospheric conditions using the available surface observations over the oceans.

The next section describes the methodology and procedures to reduce the errors in the model initial conditions and presents experiment design to test the significance of the methodology. Section 3 shows the results of the model predictions of the March 1993 superstorm with and without the improved initial conditions, as verified against available observations. Section 4 discusses the implications of the results. A summary and concluding remarks are given in the final section.

## 2. Methodology

### a. Numerical model

A mesoscale version of the RFE model (Staniforth and Mailhot 1988) is used for the present study, which is identical to that used in Huo et al. (1995). This model integrates the hydrostatic primitive equations in  $\sigma$  coordinates (23 levels in the vertical) using a semi-implicit, semi-Lagrangian temporal discretization with a 600-s time step and a finite-element spatial discretization. The computational domain is overlaid on a polar stereographic map projection true at 60°N and covers the entire Northern Hemisphere. Its lateral boundary is tangent to the equator where a solid-wall boundary con-

dition is applied. It has a uniform high-resolution (50 km) subdomain that is surrounded by a region where the resolution smoothly varies: each successive mesh length is a constant multiple of that of its preceding neighbor. The model reads the initial conditions from either the global or the regional analysis and then interpolates to its own model grid. To prevent the appearance of spurious internal gravity waves during the first 6–12 h, an implicit normal mode initialization technique (Temperton and Roch 1991) is used to adjust the mass and flow fields.

The complete set of the physical processes contained in the RFE model includes vertical turbulent fluxes of momentum, heat, and moisture, moist convection and stable condensation, solar and infrared radiation. The land surface temperature and moisture are predicted by the force–restore method (Deardorff 1978) and surface-layer exchanges of heat, moisture, and momentum are treated on the basis of similarity theory, assuming a stratified surface layer between the ground and the first model level. The SST distribution is provided by the global analysis and held constant during the model integration. A turbulent kinetic energy–based PBL scheme (Benoit et al. 1989) is used to treat the vertical turbulent transport in the PBL. The subgrid-scale deep cumulus convection is handled by the Kuo scheme while the grid-scale condensation is calculated by a stable condensation scheme, in which supersaturation is removed when relative humidity exceeds a saturation point.

### b. PV thinking

The dynamic variable, PV, has recently received considerable attention due to its properties of conservation (in the absence of diabatic heating and friction) and invertibility. It is the invertibility principle that makes the PV thinking (and doing) more attractive since one can obtain the wind and temperature fields associated with PV perturbations—the so-called piecewise PV inversion. For a fully baroclinic and compressible flow, the Ertel’s potential vorticity (EPV) is given by

$$q = \rho^{-1} \boldsymbol{\eta} \cdot \nabla \theta, \quad (1)$$

where  $\rho$  denotes the air density and  $\boldsymbol{\eta}$  and  $\theta$  are the three-dimensional absolute vorticity vector and potential temperature, respectively. EPV is a conserved quantity following motion in an inviscid flow in three dimensions (Rossby 1940; Ertel 1942). In the context of PV thinking, the cyclonic development can be described in terms of the interactions between upper- and lower-level PV anomalies as well as surface thermal anomalies (Hoskins et al. 1985; Davis 1992a). Of particular relevance to the present study is that a surface temperature anomaly can also be regarded as equivalent to a concentrated PV anomaly contained in a thin surface layer (Bretherton 1966; Hoskins et al. 1985), just like a surface charge in electrostatics. A warm (cold) surface temperature anomaly is associated with a cyclonic (anticy-

clonic) circulation in three dimensions. More importantly, three-dimensional balanced fields of the mass and winds associated with the surface thermal anomaly can be obtained through the piecewise PV inversion. It is this invertibility property that motivates us to conduct the present study. The essential ideas of the methodology are to (i) treat the 1000-hPa air temperature difference between the observed and the model initial condition as a surface PV surrogate (Reed et al. 1992); (ii) invert it to obtain the pertinent balanced wind and mass fields; and (iii) add the three-dimensional fields to the initial conditions to improve the initial representation of lower-tropospheric conditions.

Depending on different balance constraints imposed on the wind and mass fields, two kinds of piecewise PV inversion have been recently used, which include the quasigeostrophic PV (QGPV) inversion (Robinson 1988; Black and Dole 1993; Hakim et al. 1996) and EPV inversion (Davis and Emanuel 1991; Davis 1992a, 1992b). The advantage of piecewise QGPV inversion is its simplicity and absence of ambiguity; but the weakness is its inaccuracy as the Rossby number becomes large—that is, close to  $O(1)$ . In contrast, the piecewise EPV inversion proposed by Davis and Emanuel (1991) is more accurate owing to the use of Charney’s (1955) balance equation in the PV diagnostic system. This method is adopted here because we pursue more accuracy than simplicity in the present study to improve the model initial conditions.

### c. Piecewise PV inversion

The piecewise PV inversion technique developed by Davis and Emanuel (1991) is based on the assumption that the irrotational component of the wind is very small relative to the nondivergent wind, which leads to the Charney (1955) nonlinear balance equation:

$$\nabla^2 \phi = \nabla \cdot f \nabla \psi + 2m^2 \left[ \frac{\partial^2 \psi}{\partial x^2} \frac{\partial^2 \psi}{\partial y^2} - \left( \frac{\partial^2 \psi}{\partial x \partial y} \right)^2 \right], \quad (2)$$

where  $\psi$  denotes the streamfunction for the nondivergent wind,  $\phi$  is the geopotential, and  $\nabla$  and  $m$  are the two-dimensional  $(x, y)$  gradient operator and map-scale factor, respectively. If the horizontal winds in Eq. (1) are replaced by nondivergent winds, we can rewrite (1) in terms of  $\phi$  and  $\psi$ :

$$q = \frac{g\kappa\pi}{p} \left[ (f + m^2 \nabla^2 \psi) \frac{\partial^2 \phi}{\partial \pi^2} - m^2 \left( \frac{\partial^2 \psi}{\partial x \partial \pi} \frac{\partial^2 \phi}{\partial x \partial \pi} + \frac{\partial^2 \psi}{\partial y \partial \pi} \frac{\partial^2 \phi}{\partial y \partial \pi} \right) \right], \quad (3)$$

where  $\kappa = R_d/C_p$ ,  $p$  is the pressure,  $\pi = C_p(p/p_0)^\kappa$  is the Exner function and serves as our vertical coordinate. With Eqs. (2) and (3),  $\phi$  and  $\psi$  can be solved for a given distribution of PV subject to appropriate boundary con-

ditions. In the present study, Dirichlet conditions for  $\psi$  and  $\phi$  are imposed on the lateral boundaries and Neumann conditions on the top and bottom boundaries:

$$\frac{\partial \phi}{\partial \pi} = f \frac{\partial \psi}{\partial \pi} = -\theta \quad \text{at } \pi = \pi_0 \quad \text{and} \quad \pi = \pi_t,$$

where  $\pi_0$  and  $\pi_t$  are the Exner functions corresponding to 1000- and 100-hPa pressure surfaces, respectively. Once  $q$  is given,  $\phi$  and  $\psi$  can be inverted from Eqs. (2) and (3).

The piecewise PV inversion method begins by first decomposing the total field of EPV ( $q$ ), geopotential height ( $\phi$ ), and streamfunction ( $\psi$ ) into the sum of a mean ( $q_0$ ,  $\phi_0$ , and  $\psi_0$ ) and collective (i.e., volume-integrated or individual) perturbations ( $q'$ ,  $\phi'$ , and  $\psi'$ ). The collective perturbations are made up by individual anomalies  $q_n$ ,  $\phi_n$ , and  $\psi_n$ . Because of the existence of nonlinear products of  $\phi$  and  $\psi$  in Eq. (3), there is no unique way to find a relationship among the  $q_n$ ,  $\phi_n$ , and  $\psi_n$ . This issue was discussed by Davis (1992b), who investigated the discrepancies in the solutions obtained from different piecewise PV inversion methods. Because of its simplicity, a linear method is used for the present study, which is explained below. If function  $F$  is a nonlinear product of  $A$  and  $B$  ( $F = AB$ ), then one approach is to write

$$F_n = \left( A_0 + \frac{1}{2} \sum_1^n A_n \right) B_n + \left( B_0 + \frac{1}{2} \sum_1^n B_n \right) A_n, \quad (4)$$

where  $A_0$  and  $B_0$  denote the mean values of  $A$  and  $B$ . Using (4), Eqs. (2) and (3) can be rewritten in perturbation form:

$$\nabla^2 \phi_n = \nabla \cdot f \nabla \psi_n + 2m^2 \left( \frac{\partial^2 \bar{\psi}}{\partial x^2} \frac{\partial^2 \psi_n}{\partial y^2} + \frac{\partial^2 \bar{\psi}}{\partial y^2} \frac{\partial^2 \psi_n}{\partial x^2} - 2 \frac{\partial^2 \bar{\psi}}{\partial x \partial y} \frac{\partial^2 \psi_n}{\partial y \partial x} \right) \quad (5)$$

$$q_n = \frac{g\kappa\pi}{p} \left[ (f + m^2 \nabla^2 \bar{\psi}) \frac{\partial^2 \phi_n}{\partial \pi^2} + m^2 \frac{\partial^2 \bar{\phi}}{\partial \pi^2} \nabla^2 \psi_n + m^2 L(\bar{\phi}, \psi_n) + m^2 L(\bar{\psi}, \phi_n) \right], \quad (6)$$

where

$$\bar{(\quad)} = (\quad)_0 + \frac{1}{2} (\quad)'$$

$$L(A, B) = - \left( \frac{\partial^2 A}{\partial x \partial \pi} \frac{\partial^2 B}{\partial x \partial \pi} + \frac{\partial^2 A}{\partial y \partial \pi} \frac{\partial^2 B}{\partial y \partial \pi} \right). \quad (7)$$

Then, Eqs. (5)–(7) form a linear closed system for the flow perturbations  $\phi_n$  and  $\psi_n$  associated with any EPV anomaly  $q_n$ . The top and bottom boundary conditions are simply:

$$\frac{\partial \phi_n}{\partial \pi} = f \frac{\partial \psi_n}{\partial \pi} = -\theta_n \quad \text{at } \pi = \pi_0 \quad \text{and} \quad \pi = \pi_t. \quad (8)$$

We impose a homogeneous boundary condition at the lateral boundaries of the inversion domain, which covers a region of approximately 10 000 km  $\times$  10 000 km.

#### d. Procedure

The CMC archive is the main data source for the present study, from which we can retrieve the CMC global analysis and conventional meteorological observations.

To invert perturbations of EPV, normally we need to define a mean state. The mean state for the present case is defined as the time average between 0000 UTC 11 March and 0000 UTC 15 March 1993, which approximately corresponds to one synoptic-scale wave period. Given the mean state, a perturbation can be simply computed as the departure from the time average. In the present study, we intend to invert only a surface thermal anomaly that is defined by the 1000-hPa temperature difference between the original model initial field and the reanalysis of observations over the Gulf of Mexico. The pertinent procedures are described as follows.

We first initialize the RFE model with the CMC global analysis at 1200 UTC 12 March 1993 and obtain a 0-h forecast. The 0-h forecast is actually the model initial conditions and our purpose is to modify it in accordance with surface observations. As shown in Fig. 1, the 1000-hPa temperatures over the Gulf of Mexico are systematically underestimated in comparison with the surface observations. We then perform the Cressman type of objective analysis of 1000-hPa temperatures that are adjusted adiabatically from the surface observations over the Gulf of Mexico and part of the western Atlantic. A temperature difference field or thermal anomaly at 1000 hPa is obtained, as given in Fig. 2, by subtracting the model initial temperature field from the adjusted field. It is evident that the thermal anomaly is positive everywhere as a result of the underestimation of temperatures in the model initial field over the warm oceans. The next step is to invert the thermal anomaly using the piecewise PV inversion technique. Since a change of the surface temperature would lead to a change in the interior PV primarily through its vertical component (i.e., absolute vorticity times vertical  $\theta$  gradient), we have to include this change in the PV inversion process. This interior PV change is calculated by (a) inverting the surface thermal anomaly alone to obtain its associated height and wind fields; (b) adding the inverted fields to the initial conditions and recalculating the interior PV; and (c) subtracting this PV from its initial field.

Figure 3 shows the north–south vertical cross sections of the inverted flow and mass fields associated with the bottom thermal anomaly and its pertinent interior PV change. Although the thermal anomaly is a localized

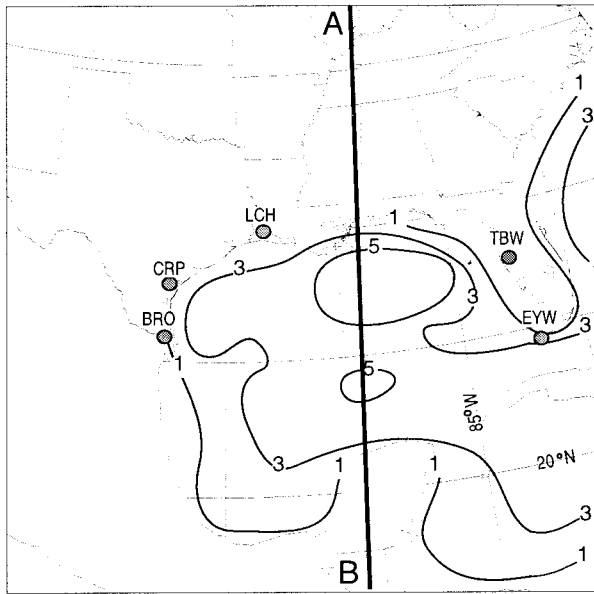


FIG. 2. Temperature difference ( $^{\circ}\text{C}$ ) at 1000 hPa between the observed (after the adiabatic adjustment) and the model initial conditions. Line *AB* denotes the location of the cross sections used in Figs. 3 and 4.

surface perturbation, its associated wind and temperature fields are three-dimensional, domain-size features. The inverted geopotential height field shows that the height deficit peaks at the surface in phase with the maximum thermal anomaly, and it decreases upward (up to 300 hPa) and away from the anomaly (Fig. 3a). Of particular significance is that the height deficit at 1000 hPa is larger than 5 dam, which amounts to a 5–6-hPa pressure fall. Similarly, the warm surface temperature anomaly, after the inversion, can extend into a deep layer, up to 500 hPa (Fig. 3b). It is evident that the deep-layer “depletion” of the mass field is hydrostatically balanced with the increase of temperature in the layer. Because of the imposed geopotential height gradients, a balanced cyclonic wind perturbation should be expected (Fig. 3c). The balanced wind perturbation is more pronounced below 800 hPa with its peak value exceeding  $10 \text{ m s}^{-1}$  at the surface. It follows that the PV inversion helps improve not only the representation of the low-level thermal field due to the upward extension of the observed surface information, but also the vertical structures of the pertinent mass and wind fields.

After obtaining the balanced mass and wind fields associated with the surface thermal anomaly, they are added to the corresponding model initial conditions. Note that the inverted low-level wind perturbation is obviously too strong since the frictional effect is not included in the PV inversion process. To roughly account for the PBL friction, we have scaled down linearly the perturbation winds in the lowest 150 hPa with decreasing pressure (e.g., 80% reduction at 1000 hPa and no change at 850 hPa); the effect of this modification

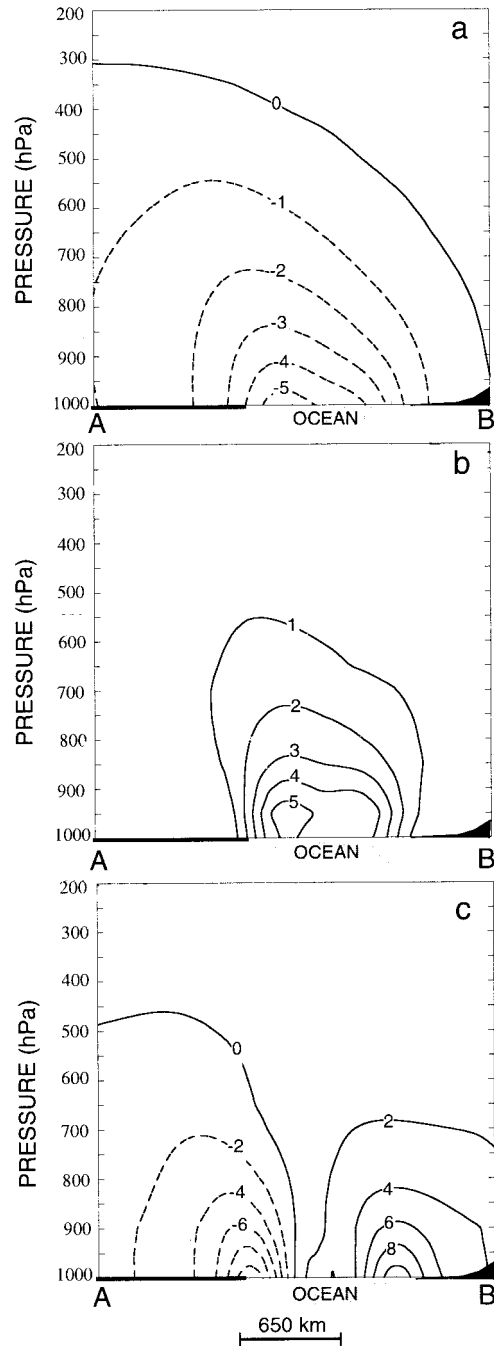


FIG. 3. Vertical cross section of the PV-inverted (a) geopotential height (dam); (b) temperature ( $^{\circ}\text{C}$ ); and (c) section-normal winds [ $\text{m s}^{-1}$ , positive (negative) values denote flows into (out of) the page] from the surface thermal anomaly and its pertinent interior PV change, which is taken along line *AB* as given in Fig. 2.

will be discussed in the next section. Since the meteorological fields being added are balanced except in the PBL, the original balances in the model initial fields would not be affected significantly. Nevertheless, the RFE model, with the modified initial conditions, will undergo the implicit normal mode initialization, before

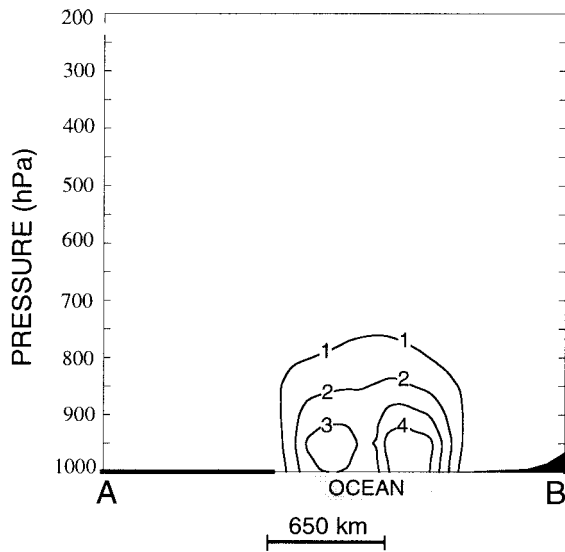


FIG. 4. Vertical cross section of the differenced specific humidity ( $\text{g kg}^{-1}$ ) in the initial conditions between EXP and EXP2 (i.e., EXP - EXP2), which is taken along line AB as given in Fig. 2.

its integration. This tends to suppress any fast-growing gravity modes, and ensures the quality of the initial wind and mass balance.

Until now we have not mentioned the impact of the modification to the initial moisture field. In the modification process, we can keep either the relative humidity or specific humidity field intact. We feel it is more appropriate to retain the original relative humidity. Therefore, this procedure increases the low-level moisture

content due to the warming of the lower atmosphere. The magnitude of the increased moisture is given in Fig. 4, which shows a maximum of approximately  $4.5 \text{ g kg}^{-1}$  at 900 hPa. Its impact on the storm development will be examined in the next section.

To see how significantly the modification procedure affects data over the neighboring areas, Fig. 5 compares the modified low-level initial conditions to the upper-air soundings taken from five stations along the coast of the Gulf of Mexico. Evidently, the modification does not seriously “contaminate” the model initial conditions in data-dense regions. Figure 6 shows the modified initial 1000-hPa temperature and SLP fields, as verified against the observed SLP. A comparison between Figs. 6 and 1 reveals that both the SLP and 1000-hPa temperature fields are much closer to the observed after the modification. Several features in Fig. 6 may potentially contribute to the initial rapid development of the storm. First, the low-level baroclinicity along the southern coast of the United States is enhanced markedly with the modified low-level thermal field, suggesting an increase in the system’s available potential energy. Furthermore, the resulting decrease in the low-level static stability will assist the deepening of the storm through both dry dynamics and enhanced moist convection. Second, an incipient cyclone with stronger absolute vorticity is initialized in comparison with that in the original model initial conditions. According to Gyakum et al. (1992), the initial intensification rate of a cyclone is directly proportional to its absolute vorticity for given surface convergence. Third, the initial storm center is brought back to the observed position, which is closer

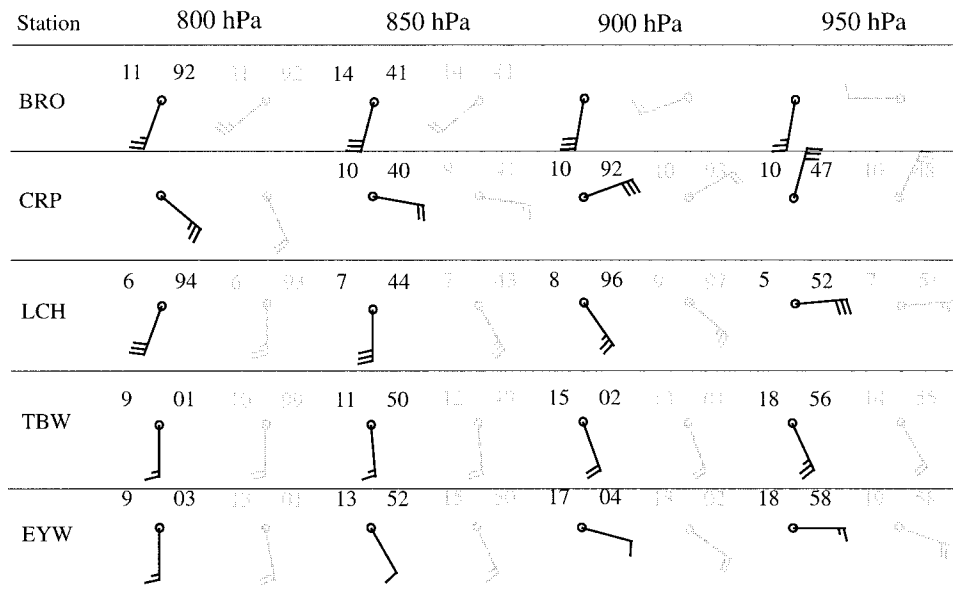


FIG. 5. Comparison of the low-level station observations (dark) with the model soundings in the modified initial conditions (light); plotted are temperature (upper left,  $^{\circ}\text{C}$ ), geopotential height (upper right, dam; first digit omitted), and horizontal winds (a full barb is  $5 \text{ m s}^{-1}$ ). Locations of the stations are given in Fig. 2.

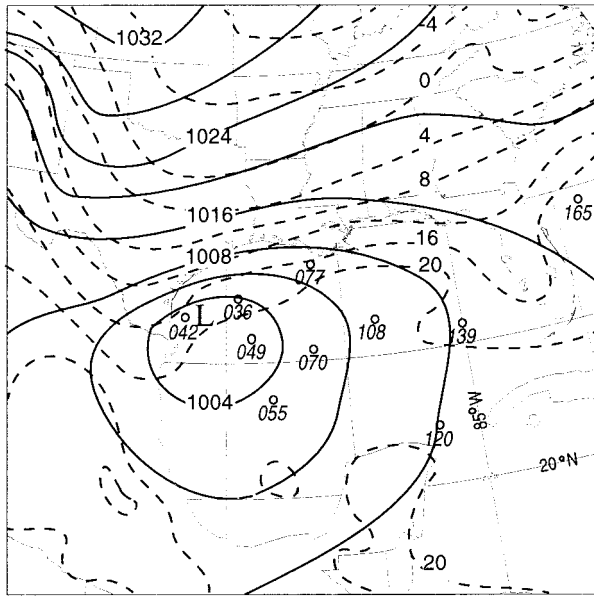


FIG. 6. As in Fig. 1 but for the modified initial conditions. Note that the observed sea level pressures are given as the excess over 1000 hPa, e.g., 049—1004.9 hPa.

to the enhanced baroclinic zone. Finally, the enhanced low-level moisture content will increase the potential of latent heat release, which could be instrumental in the development of the prefrontal squall line and its associated quantitative precipitation; they were poorly predicted by the then-operational models. As will be clear later, the enhanced low-level moisture content plays the most important role in the storm's incipient stage.

#### e. Experiment design

In the preceding subsection, we have demonstrated that the model initial conditions over data-sparse regions could be improved through the piecewise PV inversion of surface thermal anomalies. A natural question is: How significant is the modification in the prediction of the March 1993 superstorm? For this purpose, we conducted a series of 36-h runs using the RFE model (Table 1). For the control run (CTL) and the sensitivity experiment (EXP), the RFE model is initialized, respectively, with the original model initial conditions and the modified initial conditions. The comparison of CTL and EXP will reveal the overall impacts of the modification on the numerical prediction of the superstorm. To separate the effects of diabatic heating from dry adiabatic processes, two additional model integrations corresponding to the respective CTL and EXP initial conditions are performed, in which neither convective parameterization nor grid-scale precipitation is allowed; they are referred to as the control-dry (CTLD) and the sensitivity-dry (EXPD), respectively. EXP1 is designed to test the sensitivity of model prediction to the changes of the initial low-level wind fields, in which the inverted

TABLE 1. Experiment design.

Code	Remarks
CTL	Control simulation with the original initial conditions.
CTLD	Same as CTL except that no latent heating is allowed.
EXP	Same as CTL except with the modified initial conditions. Original <i>relative humidity</i> is retained and the low-level perturbation winds are scaled down linearly with decreasing pressure.
EXPD	Same as EXP except with no latent heating.
EXP1	Same as EXP except that the low-level perturbation winds are not scaled down.
EXP2	Same as EXP except with the original <i>specific humidity</i> retained.
EXP3	Same as CTL except with the modified temperatures in the lowest 100 hPa at the initial time.

low-level perturbation winds are not scaled down. As shown in the previous subsection, the low-level moisture content is also increased when we increase the temperature without modifying the initial relative humidity. To isolate the effects of the increased low-level moisture content on the storm development, EXP2 is run with the same initial conditions as EXP except that the original specific humidity is used. Finally, the impact of including alone the adiabatically adjusted thermal field is examined in EXP3, in which the corrected surface temperatures are used to obtain temperatures at 1000 and 950 hPa by assuming a dry- (moist-) adiabatic lapse rate in regions with relative humidity less than 80% (>80%).

### 3. Results

The storm tracks and time series of the central SLP are shown in Figs. 7 and 8 for the observation, CTL, and various sensitivity experiments. Before discussing the best simulation (i.e., EXP), let us examine first the effects of the improved temperature analysis in the PBL on the storm development (EXP3). It is evident from Fig. 8 that only slight improvement in the deepening rate occurs during the first 12-h integration compared to that in CTL; similarly for the track (not shown). These improvements are almost negligible when comparing CTL and EXP. Therefore, the benefits from the simply improved PBL thermal structures are rather limited.

By comparison, EXP predicts the track of the storm better than that in CTL, especially in the first 12 h (Fig. 7). Of interest is that although the cyclone center in CTL is initially displaced about 400 km to the southwest of the observed, it is adjusted to the observed position after the 12-h integration. This appears to be mainly determined by upper-level forcings, namely, the approach of two short-wave troughs with intense PV concentrations traveling in a larger-scale cyclonic circulation (see Huo et al. 1995; Kocin et al. 1995). The presence of the Appalachian Mountains and the cold-air damming along its east side contribute little to the track

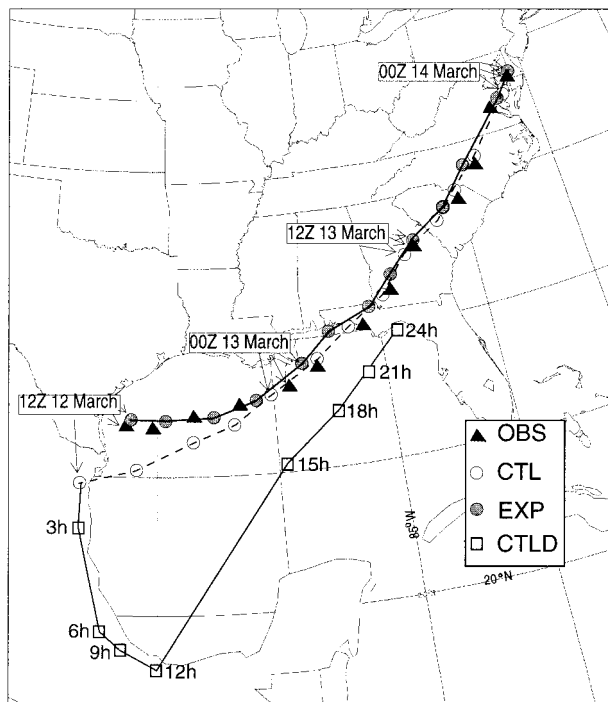


FIG. 7. The tracks of the superstorm from the observed (triangle), the control run (open circle), the experiment run (shaded circle), and the dry control run (open square).

(not shown), as found from a sensitivity experiment in which everything is kept identical to that in EXP except for the removal of the Appalachians.

It is clear that EXP also predicts well the storm's early deepening over the ocean during the first 18-h integration, with a 16-hPa central pressure fall compared to the observed 17 (14) hPa from the NCEP (CMC) surface analysis (Fig. 8). In contrast, the CTL run underpredicts substantially the early development of the storm—that is, by 10 hPa—when it is located over the ocean. In particular, the CTL storm fails to deepen in the first 6 h—a typical spinup problem in NWP models. As mentioned previously, several factors in the model initial conditions could account for the underprediction and the initial slow spin up. They include the weaker baroclinicity along the south coast, the stronger static stability in the lower troposphere, the weaker storm-scale cyclonic circulation, the southwest shift of the storm center with respect to the baroclinic zone, and most importantly, the lower moisture content in the maritime boundary layer, which have been all modified either directly or indirectly. Note, though, that EXP could not predict correctly the deepening rate of the storm in the second half of the 36-h integration—that is, with an underestimation of 3–5 hPa (18 h)<sup>-1</sup> (Fig. 8). This appears to be caused by the approaching of the two upper-level short-wave troughs that may not be very well defined in the model initial conditions when they are located over the data-sparse Rocky Mountains and northern Mexico at 1200

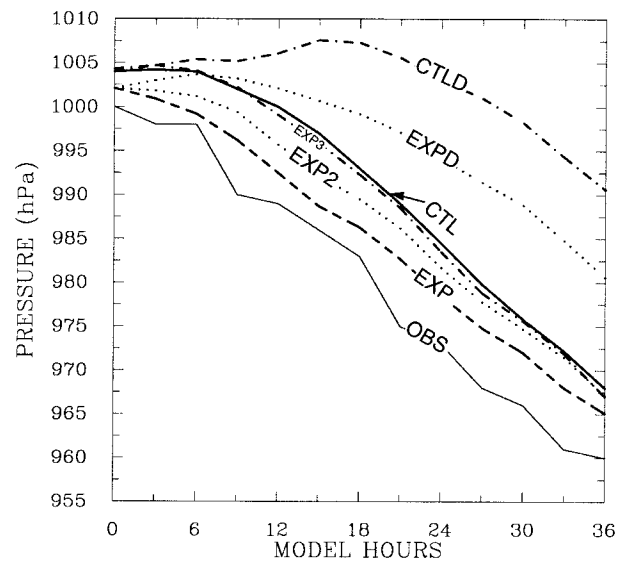


FIG. 8. The time series of the superstorm's central SLP from the observed (thin solid), the control (thick solid), and sensitivity runs.

UTC 12 March 1993. Nevertheless, the final intensity of the storm in EXP is better predicted than that in CTL. Subsequently, the differences in the track and intensity of the storm between the two runs decrease with time (not shown). This is again attributable to the dominant roles of the two upper-level short-wave troughs as they approach the east coast (Huo et al. 1995). It should be mentioned that the then operational forecasts were very similar in many aspects to the CTL cyclogenesis, which could capture the explosive deepening on 13 March but all failed to predict the early rapid deepening of the storm on 12 March when it was crossing the Gulf of Mexico (Kocin et al. 1995).

Figure 9 compares the structures and evolution of the low-level baroclinicity, as denoted by the 500–1000-hPa thickness, as well as its impact on the storm development between CTL, EXP, and the CMC analysis (ANA). The initial 500–1000-hPa thickness field, after being modified, exhibits stronger baroclinicity along the south coast of the United States, just as the 1000-hPa isotherms (cf. Figs. 1 and 6). Once the model is integrated forward, the enhanced baroclinic zone tends to be advected cyclonically into the northeast–southwest orientation at 12 h (see Fig. 9b) and the half-circular shape at 24 h (see Fig. 9e), as indicated by shadings. The thickness isopleths associated with the baroclinic zone in EXP always show stronger gradients than those in CTL (cf. Figs. 9a,b and Figs. 9d,e), and they conform more closely to the CMC analysis (cf. Figs. 9b,c and Figs. 9e,f).

Likewise, EXP predicts the structure and central SLP of the cyclone better than those in CTL, as verified against the CMC analysis. In particular, EXP reproduces very well the general asymmetry of the cyclone, the strong pressure gradients or cyclonic flows to the north

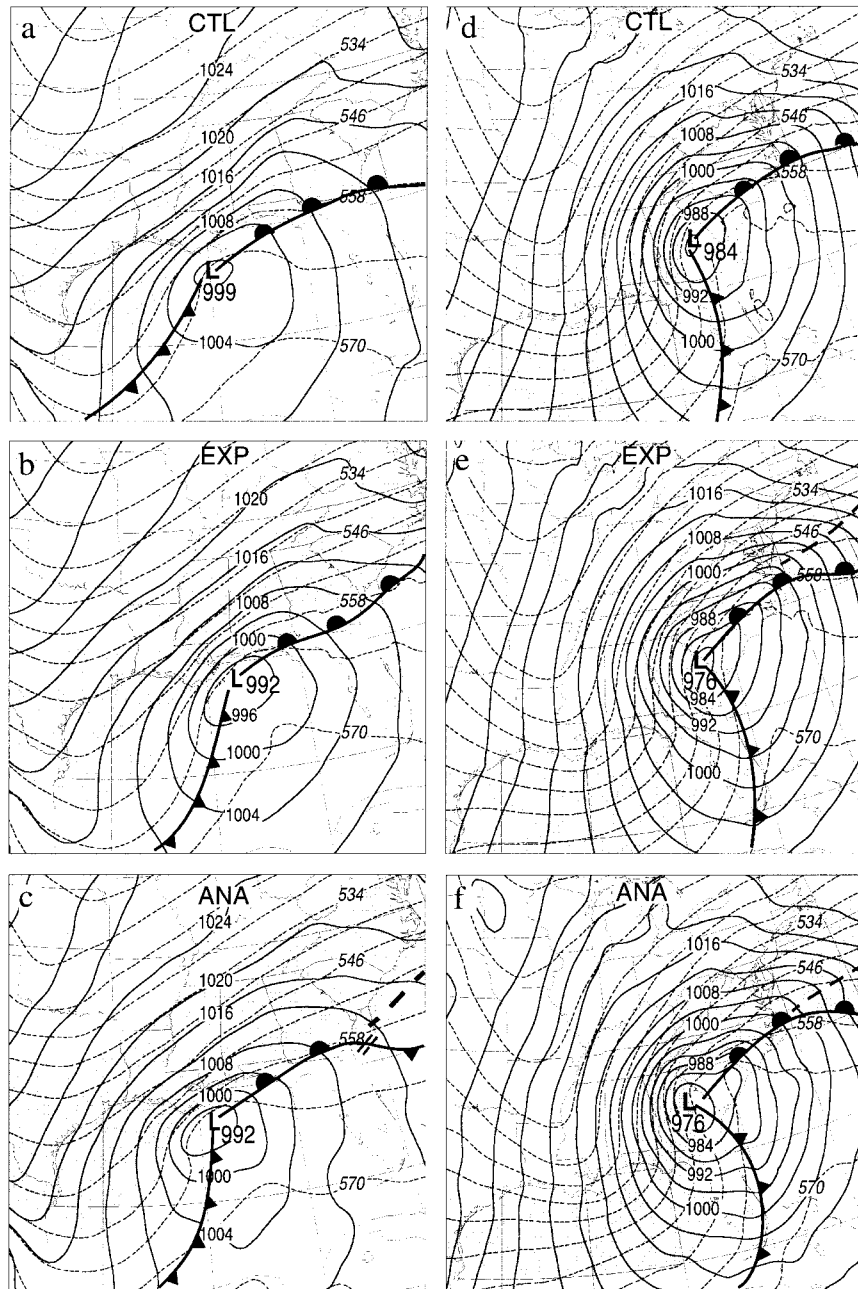


FIG. 9. Horizontal map of SLP (solid) at intervals of 4 hPa and 500–1000-hPa thickness (dashed) at intervals of 6 dam from the 12-h (left column) and 24-h (right column) integrations of the control run (CTL, upper panel), the experiment run (EXP, middle panel), and the CMC analyses (ANA, bottom panel), which are valid at 0000 and 1200 UTC 13 March 1993, respectively. The area between 558- and 534-dam thickness isopleths is shaded to indicate the average baroclinicity in the 500–1000-hPa layer.

and east of the cyclone, as well as the positions of the warm- and cold-frontal troughs. Thus, the EXP cyclone shows more intense thermal advection ahead of the warm front or in the warm sector, implying the increased transport of high- $\theta_e$  air from the tropical region. When the effect of diabatic heating is considered, a positive

feedback process should be operative in the rapid deepening of the storm (Kuo et al. 1991; Huo et al. 1995).

The modified initial conditions also have an important impact on the development of the prefrontal squall line. Figure 10 shows the predicted pattern of precipitation rates from 12-h integration of the CTL and EXP runs,

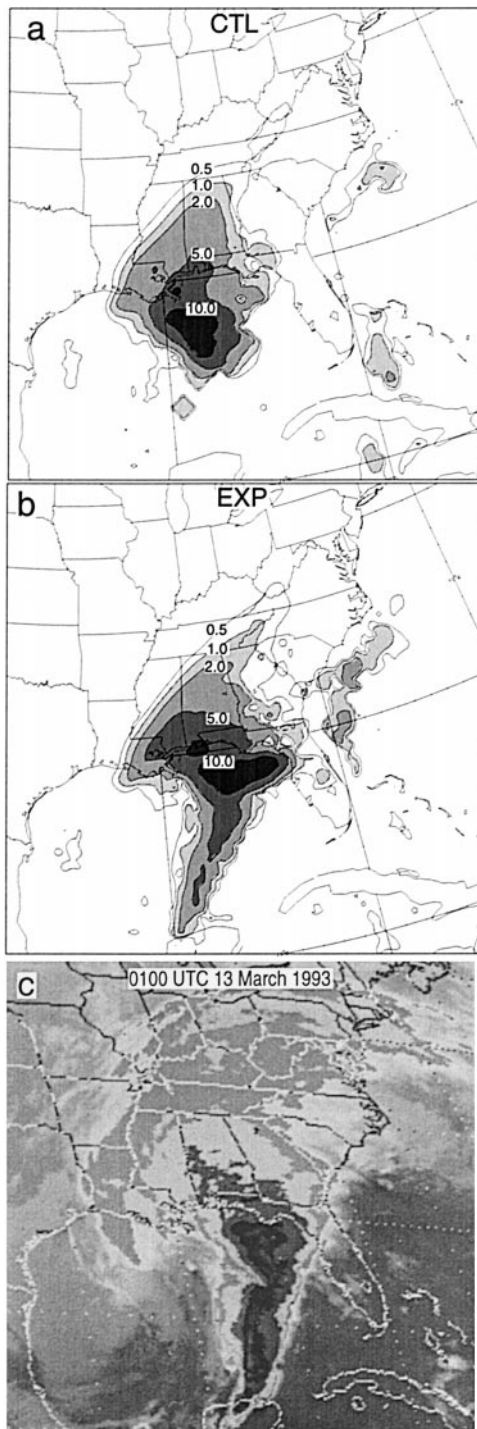


FIG. 10. Horizontal map of precipitation rates ( $\text{mm h}^{-1}$ ) from the 12-h integration of the control run (CTL, upper panel) and the experiment run (EXP, middle panel), which are valid at 0000 UTC 13 March 1993. Bottom panel shows satellite imagery at 0100 UTC 13 March 1993.

as compared to the infrared satellite imageries at nearly the same time. Satellite imagery at 0100 UTC 13 March shows a comma-shaped pattern of cloudiness associated with the cyclone with a well-developed squall line occurring ahead of the cold front (Fig. 10c). Radar summaries also display some areas of less organized precipitation over the eastern United States that was associated with the warm front (see Fig. 5d in Huo et al. 1995). It is clear that the 12-h CTL forecast fails to produce the initial development of the prefrontal squall line (cf. Figs. 10a and 10c), whereas EXP replicates very well the structure and orientation of the prefrontal squall system and the reduced precipitation in the vicinity of the warm front (Fig. 10b). Apparently, the reasonable prediction of the squall line could be attributed to the improved initial thermal and moisture fields in the lower troposphere, since the increased  $\theta_e$  air in the boundary layer makes it easy to tap the CAPE that is crucial to the development of deep convection along the cold front.

Because of the presence of pronounced surface heat and moisture fluxes over the warm ocean, the maritime boundary layer in CTL is gradually recovered after the 12-h integration (not shown). Thus, the CTL prediction could reproduce reasonably, as does the EXP prediction, the development of the squall line at the end of 24-h integration (not shown). Nevertheless, the CTL-predicted squall line is not as well organized as the observed and the EXP-predicted squall line. The underprediction in CTL is attributable to the lack of organized baroclinic forcing along the cold front, in addition to the lack of sufficient CAPE.

The results of EXP1 are very similar to that of EXP (not shown). An examination of the low-level winds shows that the PBL processes dampen rapidly the excessively strong low-level winds. After 3-h integration, the low-level winds in EXP1 are almost identical to that in EXP. There are also little notable differences in other fields. It follows that the downward scaling of the initial low-level perturbation winds has little impact on the storm development. The PBL wind field appears to be determined primarily by the mass field and surface frictional effect.

While scaling down the perturbation winds in the PBL has little effect on the storm development, the impact of modifying the low-level perturbation moisture, as given in Fig. 4, is significant. For example, when the CTL specific humidity field is used in the EXP initial condition (EXP2), it results in a marked decrease in the initial deepening of the storm (Fig. 8), only  $3 \text{ hPa}$  ( $9 \text{ h}$ ) $^{-1}$  compared to  $6 \text{ hPa}$  ( $9 \text{ h}$ ) $^{-1}$  in the EXP run. As expected, much less precipitation occurs in EXP2 than in EXP along the storm track (Fig. 11) because there is less low-level moisture content and consequently less CAPE. Nevertheless, the EXP2 storm track is almost the same as that of EXP since it is determined mainly by dry dynamics. The result reveals that the latent heating is essential in the initial deepening of the storm.

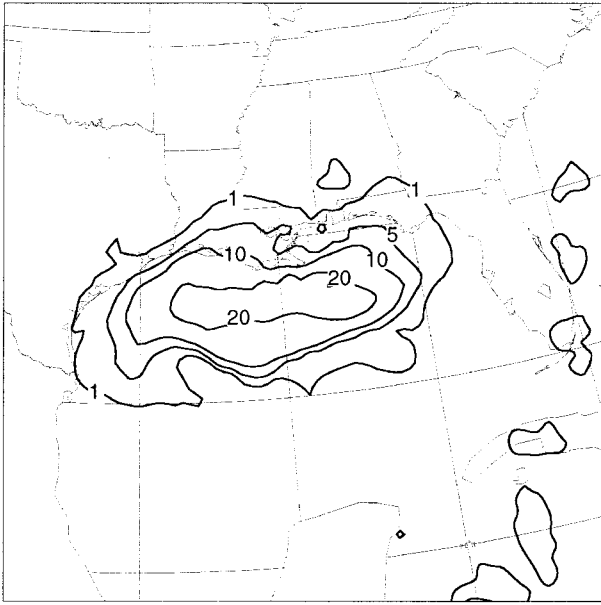


FIG. 11. The difference of 9-h accumulated precipitation (mm) between EXP and EXP2 (i.e., EXP - EXP2), valid at 2100 UTC 12 March 1993.

To gain further insight into the importance of latent heat release in the storm development, the CTL and EXP runs are compared with their dry counterparts, CTLD and EXPD. When the latent heat release is removed, the EXPD storm follows a track similar to that in EXP and to the observed except that the dry cyclone is slower (not shown), whereas the CTLD cyclone follows a track that departs markedly from the observed in the first 12-h integration (Fig. 7). Specifically, the CTLD storm goes first southward along the Gulf Coast to Veracruz of Mexico, and then it moves northeastward and begins to catch up with its moist counterpart by 18 h into the integration. Subsequently, the two tracks converge and follow closely the observed. These different tracks show that the early cyclone movement is sensitive to how well the low-level cyclonic circulations and moisture are defined when the influence of the upper-level forcing is weak. The storm movement is usually determined by large-scale dry dynamics. When the large-scale forcing is weak during the early stage of development, the diabatic heating plays an important role in putting the storm on the right track. A comparison of the central SLP traces (Fig. 8) between the dry (i.e., CTLD and EXPD) and the moist runs (i.e., CTL and EXP) further shows the importance of latent heat release in the early rapid spin-up of the storm. In particular, the CTLD storm does not deepen at all during the first 15 h when it meanders around the Gulf of Mexico. Similarly, even with the improved low-level cyclonic circulation, EXPD fails to produce significant deepening of the cyclone during the same period. These two dry simulations results are consistent with each other since the added fields in EXPD are equivalent barotropic in the vertical. Nevertheless,

the two dry runs reproduce reasonably well the cyclone's deepening rate at later stages when the upper-level short-wave troughs propagate toward the East Coast region. Despite the similar deepening rates, the cyclone's final intensity in EXPD is always stronger than that in CTLD due to the initially added perturbations.

#### 4. Discussion

During the past decades, considerable effort has been spent on the improvement of the model initial conditions (Bengtsson 1990), since the short-range NWP is, to a certain extent, an initial value problem. To improve the quality of the model initial conditions, numerous operational NWP centers around the world have developed various types of four-dimensional data assimilation (FDDA) systems, which contributed much to the recent progress in the short-range NWP. However, observations are a prerequisite for any FDDA system. Over places where conventional upper-air and surface observations are lacking, such as over oceans or remote regions, the use of a FDDA system may not be able to significantly increase the forecast skill. If a NWP model is initialized with these analyses, it would either "reject" the possible unbalanced surface data or "forget" the surface information once it is integrated. Obviously, these surface observations contain valuable information in the context of the air-sea interaction and in some cases the air-land interaction, as demonstrated in this study. The surface information may be extremely important during significant weather events such as the superstorm of March 1993 (Gilhousen 1994). However, these surface observations could only play very limited roles in the short-range NWP, because of the lack of an efficient way to incorporate them into the model initial conditions.

The methodology proposed in this study represents an attempt to improve the model initial conditions by applying the piecewise PV inversion technique to available surface observations over ocean. The essence of this approach is to improve the model initial fields by extending the surface information into a deep layer in a dynamically consistent manner. Since the inverted mass and wind fields are in dynamic and thermodynamic balance, it would have little effect on the existing balanced states in the original system. It should be mentioned that this approach has been shown by Wang (1995) to be more successful in obtaining a numerical simulation of an East Coast frontal cyclogenesis case as documented by Bosart and Sanders (1991), after the lower-tropospheric conditions over the western Atlantic Ocean were improved with available surface information. Certainly, more case studies are needed to determine the significance of this approach in the improvement of model initial conditions as well as short-range NWP and quantitative precipitation forecasts.

It should be mentioned that the methodology proposed herein may be case dependent, which is more related to the piecewise PV inversion technique itself.

Specifically, because Eqs. (2) and (3) are nonlinear equations, there is no unambiguously correct way to perform the piecewise EPV inversion (see Davis 1992b). Furthermore, the final solution of the inverted fields is often sensitive to the definition of a mean state, the use of different boundary conditions and the domain size. Nonetheless, Davis' (1992b) diagnostics show that the relative differences between various inversion methods are generally less than 25% even for flows with large Rossby number. Another concern is associated with the basic assumptions involved in the PV inversion—namely, the neglect of (i) the irrotational component of the flow and (ii) the frictional effect in the boundary layer. The first assumption may not be realistic for mesoscale convective weather systems, such as fronts, squall lines, and mesoscale cloud clusters, in which the divergent component is intense. The neglect of friction is apparently unrealistic. But a sensitivity experiment with the low-level perturbation winds scaled down to account for the frictional effect shows that the instantaneous neglect of it does not have any significant influence on the prediction of the storm.

Finally, this methodology could be criticized due to the generation of the domain size perturbations as a result of the use of Laplacian operators in the piecewise PV inversion. Specifically, the height and wind perturbation appear to have “contaminated” the cyclone structure over the data-rich regions, as shown in Figs. 3a,c. This “contamination” is small in the present case; but it could be significant for weak gradient background flows. Thus, the present study serves only as an introduction of the method and demonstrates how it can be applied to a particular storm. Further studies are needed to improve this methodology and to examine the validity of the technique in a variety of cases.

## 5. Summary and conclusions

In this study, a methodology has been developed to improve the model initial conditions, based solely on available surface temperature observations. It is then tested with the numerical prediction of the March 1993 superstorm that is initialized at the storm's very incipient stage over the Gulf of Mexico, using the Canadian RFE model. In this methodology, we make use of the Davis piecewise PV inversion technique and treat the model temperature errors at the lowest boundary (i.e., 1000-hPa level) as a surrogate PV anomaly. After the wind and mass fields are inverted from the surface thermal anomaly and its pertinent interior PV anomaly, the three-dimensional, dynamically consistent set of meteorological fields are added to the original model initial conditions to improve the low-level representation of the atmosphere.

It is demonstrated that this methodology provides a better set of initial conditions for the prediction of the March 1993 superstorm when it was located over the data-sparse Gulf of Mexico. Specifically, the modified

initial conditions exhibit significant improvements in the low-level baroclinicity along the southern coast of the United States, in the low-level static stability over the Gulf of Mexico, in the initial cyclonic circulation and intensity of the storm, and in the initial position of the storm center as well as the low-level moisture content or CAPE in the warm sector. Consequently, the RFE model reproduces very well the early rapid deepening and track of the storm over the ocean, the development of a prefrontal squall line and the associated quantitative precipitation, the traces of the storm's central SLP, and the intensity of the pertinent cyclonic flows during the life cycle of the cyclone, as verified against the CMC analysis and other available observations. By comparison, the model without the modification predicts poorly the above-mentioned features. The results reveal that the methodology proposed herein is promising in the improvement of the model initial conditions based on available surface observations.

*Acknowledgments.* We are very grateful to Dr. Chris Davis for providing us with the PV inversion programs, and to Dr. Gary Lackmann for his helpful discussions. This research was supported by “Fonds pour la Formation de chercheurs” (FCAR) of the province of Quebec, and the Atmospheric Environment Service (AES) of Environment Canada. The first author (Z. Huo) was also supported by a graduate scholarship from FCAR.

## REFERENCES

- Anthes, R. A., Y.-H. Kuo, and J. R. Gyakum, 1983: Numerical simulations of a case of explosive cyclogenesis. *Mon. Wea. Rev.*, **111**, 1174–1188.
- Bengtsson, L., 1990: Advances in numerical prediction of the atmospheric circulation in the extratropics. *Extratropical Cyclones: The Erik Palmén Memorial Volume*, C. Newton and E. Holopainen, Eds., Amer. Meteor. Soc., 193–220.
- Benoit, R., J. Cote, and J. Mailhot, 1989: Inclusion of a TKE boundary layer parameterization in the Canadian regional finite-element model. *Mon. Wea. Rev.*, **117**, 1726–1750.
- Black, R. X., and R. M. Dole, 1993: The dynamics of large-scale cyclogenesis over the North Pacific Ocean. *J. Atmos. Sci.*, **50**, 421–442.
- Bosart, L. F., and F. Sanders, 1991: An early-season coastal storm: Conceptual success and model failure. *Mon. Wea. Rev.*, **119**, 2831–2851.
- Bretherton, F. P., 1966: Critical layer instability in baroclinic flows. *Quart. J. Roy. Meteor. Soc.*, **92**, 325–334.
- Canadian Meteorological Center, 1995: *CMC Reference Guide*. Canadian Meteorological Center, 316 pp. [Available from CMC, Environment Canada, 2121 Trans-Canada Highway, Downsview, ON M3H 5T4, Canada.]
- Charney, J. G., 1955: The use of primitive equations of motion in numerical prediction. *Tellus*, **7**, 22–26.
- Davis, C. A., 1992a: A potential-vorticity diagnosis of the importance of initial structure and condensational heating in observed extratropical cyclogenesis. *Mon. Wea. Rev.*, **120**, 2409–2428.
- , 1992b: Piecewise potential vorticity inversion. *J. Atmos. Sci.*, **49**, 1397–1411.
- , and K. A. Emanuel, 1991: Potential vorticity diagnostics of cyclogenesis. *Mon. Wea. Rev.*, **119**, 1929–1953.
- Doward, J. W., 1978: Efficient prediction of ground surface tem-

- perature and moisture with inclusion of a layer of vegetation. *J. Geophys. Res.*, **83**, 1889–1903.
- Ertel, H., 1942: Ein neuer hydrodynamischer Wirbelsatz. *Meteor. Z.*, **59**, 277–281.
- Gilhousen, D. B., 1994: The value of NDBC observations during March 1993's "storm of the century." *Wea. Forecasting*, **9**, 255–264.
- Gyakum, J. R., P. J. Roebber, and T. A. Bullock, 1992: The role of antecedent vorticity development as a conditioning process in explosive cyclone intensification. *Mon. Wea. Rev.*, **120**, 1465–1489.
- Hakim, G. J., D. Keyser, and L. F. Bosart, 1996: The Ohio Valley wave-merger cyclogenesis event of 25–26 January 1978. Part II: Diagnosis using quasigeostrophic potential vorticity inversion. *Mon. Wea. Rev.*, **124**, 2176–2205.
- Hoskins, B. J., M. E. McIntyre, and R. W. Robertson, 1985: On the use and significance of isentropic potential vorticity amps. *Quart. J. Roy. Meteor. Soc.*, **111**, 877–946.
- Huo, Z., D.-L. Zhang, J. R. Gyakum, and A. N. Staniforth, 1995: A diagnostic analysis of the superstorm of March 1993. *Mon. Wea. Rev.*, **123**, 1740–1761.
- Kocin, P. J., P. N. Schumacher, R. F. Morales, and L. W. Uccellini, 1995: Overview of the 12–14 March 1993 superstorm. *Bull. Amer. Meteor. Soc.*, **76**, 165–182.
- Kuo, Y.-H., M. A. Shapiro, and E. G. Donall, 1991: Interaction of baroclinic and diabatic processes in numerical simulations of a rapid developing marine cyclone. *Mon. Wea. Rev.*, **119**, 368–384.
- Reed, R. J., M. T. Stoelinga, and Y.-H. Kuo, 1992: A model-aided study of the origin and evolution of the anomalously high potential vorticity in the inner region of a rapidly deepening marine cyclone. *Mon. Wea. Rev.*, **120**, 893–913.
- Robinson, W. A., 1988: Analysis of LIMS data by potential vorticity inversion. *J. Atmos. Sci.*, **45**, 2319–2342.
- Rosby, C. G., 1940: Planetary flow patterns in the atmosphere. *Quart. J. Roy. Meteor. Soc.*, **66** (Suppl.), 68–87.
- Staniforth, A. N., and J. Mailhot, 1988: An operational model for regional weather forecasting. *Comput. Math. Appl.*, **16**, 1–22.
- Temperton, C., and M. Roch, 1991: Implicit normal mode initialization for an operational regional model. *Mon. Wea. Rev.*, **119**, 667–677.
- Wang, J., 1995: A numerical investigation of the coastal frontal cyclogenesis of 3–4 October 1987. M.S. thesis, McGill University, 79 pp. [Available from the Dept. of Atmospheric and Oceanic Sciences, McGill University, Montreal, PQ H3A 2K6, Canada.]
- Zhang, D.-L., and J. M. Fritsch, 1986: Numerical simulation of the meso- $\beta$ -scale structure and evolution of the 1977 Johnstown flood. Part I: Model description and verification. *J. Atmos. Sci.*, **43**, 1913–1943.